Pergamon

Int. J. Heat Mass Transfer. Vol. 41, No. 13, pp. 1929–1944, 1998

Printed in Great Britain
0017-9310/98 $19.00+0.00

PII: S0017-9310(97)00315-3

Kinetic theory analysis of heat transfer in granular flows

V. V. R. NATARAJAN and M. L. HUNT†

Division of Engineering and Applied Sciences, California Institute of Technology, Pasadena, CA 91125, U.S.A.

(*Received* 21 *March* 1997 *and in final form* 6 *October* 1997)

Abstract—Based on a dense-gas kinetic theory model, theoretical solutions were generated to study and compare experimental and theoretical results for velocity profiles and heat transfer characteristics in granular flows in a vertical chute. The results indicated good agreement between theoretical and experimentally measured mean velocity profiles but the magnitude of the fluctuation velocities were underpredicted by the theoretical solutions. Qualitative agreement was found between experimental and theoretical results for convective heat transfer. The results indicated that particle size and the medium density adjacent to the boundary played an important role in determining the heat transfer at the boundary.

INTRODUCTION

Over the past two decades, significant efforts have been made to describe the flows of granular materials in terms of concepts borrowed from dense-gas kinetic theory [1]. While a granular flow has an overall bulk motion, the individual particles making up the material may collide, roll or slide against each other, and may interact with the bounding surfaces. Hence, the individual particle motions are composed of a mean component and a fluctuating, or random component. An analogy is drawn between this random motion and the random motion of molecules in a dense gas. Ogawa [2] used the term 'granular temperature' to quantify the random motions of particles about the mean velocity. The granular temperature is defined as the average of the sum of the squares of the three fluctuating velocity components. Since the granular temperature is a measure of the specific random kinetic energy of the flow, it replaces the thermodynamic temperature in the dense-gas kinetic theory based analysis of rapid granular flows. However, significant differences exist between the interactions amongst gas molecules in a dense gas and particles in a granular flow. Unlike the collisions between molecules, the collisions between granular particles are inelastic and always involve a dissipation of the random kinetic energy. Hence, in order to sustain the flow, it is necessary to supply energy to the system, either through shear work or through vibration. These analogies between dense gases and granular flows are expected to be valid in the 'rapid granular flow' regime, characterised by high shear rates and low to moderately high solid fractions in the flows [3].

As in the case of dense gases, the transport phenomena in the rapid granular flow regime are determined by two mechanisms. The first is the streaming, or kinetic, mode which accounts for the transport of particle properties as the particles move freely across void spaces in the flows. The second mechanism is the collisional mode, which accounts for transfer of momentum during collisional interactions between particles. The kinetic mode is dominant at low solid fractions because the particles can 'stream' over longer distances. The collisional mode dominates at higher solid fractions as the increased proximity of particles increases the frequency of collisions.

Savage and Jeffrey [4] and Jenkins and Savage [5] were responsible for the initial development of constitutive models for granular flows based on dense-gas kinetic theory. They derived integral forms for the stress and fluctuation energy flux due to the collisional interactions between the particles. Lun *et al.* [6] used elements of the Chapman–Enskog dense-gas kinetic theory (Chapman and Cowling [1]) to develop the kinetic theory for granular flows of slightly inelastic particles. Both collisional and streaming modes of transport were included, enabling the theory to be extended to dilute systems as well. Furthermore, Lun *et al.* [6] recognized that the presence of gradients in the velocity, density and granular temperature profiles in a rapid granular flow meant that the system was not in an equilibrium state and hence could not be described by a Maxwellian velocity distribution function. They were successful in incorporating a first order correction for the velocity distribution function, though it entailed an assumption of collisional isotropy. Several other works refined and extended the kinetic theory treatment to treat a variety of particle properties and flow conditions [7–13]. The constitutive models based on dense-gas kinetic theory are more

† Author to whom correspondence should be addressed.

NOMENCLATURE

A	dimensionless channel half-width
Bi	Biot number
c_{air}	specific heat of air, at constant pressure [W s (kg °C)$^{-1}$]
c_p	specific heat of particle [W s (kg °C)$^{-1}$]
e_p	particle–particle coefficient of restitution
e_w	particle–wall coefficient of restitution
$\mathbf{F}$	specific body force [N m^{-3}]
$\boldsymbol{g}$	acceleration due to gravity [m s^{-2}]
g_0	radial distribution function
h	mean heat transfer coefficient [W (m^2 °C)$^{-1}$]
h_{wp}	wall–particle heat transfer coefficient [W (m^2 °C)$^{-1}$]
$\mathbf{I}$	identity matrix
k_c	thermal conductivity of assembly at critical density [W (m °C)$^{-1}$]
k_g	thermal conductivity of interstitial gas [W (m °C)$^{-1}$]
k_{kt}	streaming thermal conductivity [W (m °C)$^{-1}$]
k_{mc}	effective molecular conductivity [W (m °C)$^{-1}$]
k_p	thermal conductivity of particle [W (m °C)$^{-1}$]
k_s	thermal conductivity of solid material [W (m °C)$^{-1}$]
k_{tol}	total thermal conductivity $k_{mc}+k_{kt}$ [W (m °C)$^{-1}$]
$\mathbf{n}$	unit normal vector directed from the wall into the flow
Nu^*	modified Nusselt number
$\mathbf{P}$	total stress tensor [N m^{-2}]
Pe^*	modified Peclet number
q_h	diffusive heat flux [W m^{-2}]
$\mathbf{S}$	deviatoric part of the rate of deformation tensor [s^{-1}]
t	time [s]
$\mathbf{T}$	granular temperature [m^2 s^{-2}]
$\mathbf{T}^*$	dimensionless granular temperature
T	thermodynamic temperature [°C]
$T_{\sigma/2}$	granular temperature at a distance of half a particle diameter from the wall [m^2 s^{-2}]
$\mathbf{u}$	mean velocity [m s^{-1}]
u_{sl}	slip velocity [m s^{-1}]
u_i'	fluctuation velocity in direction 'i' [m s^{-1}]
u_x	mean streamwise velocity [m s^{-1}]
$u_{x-\sigma/2}$	mean streamwise velocity at a distance of half a particle diameter from the wall [m]
u_x^*	dimensionless mean streamwise velocity
u_y'	transverse fluctuation velocity [m s^{-1}]
W	channel half-width [m]
X	dimensionless streamwise coordinate
Y	dimensionless transverse coordinate.

Greek symbols

α_c	thermal diffusivity of assembly at critical density [m^2 s^{-1}]
γ	specific fluctuation energy dissipation [kg m s^{-3}]
Γ	flux of fluctuating energy [kg s^{-3}]
ν	solid fraction
ν^*	maximum shearable solid fraction for a particle assembly
$\nu_{\sigma/2}$	solid fraction at a distance of half a particle diameter from the wall
ρ	bulk density of material [kg m^{-3}]
ρ_{air}	density of air [kg m^{-3}]
ρ_p	particle density [kg m^{-3}]
σ	particle diameter [m]
ϕ'	specularity coefficient
χ	thermal resistance of interstitial fluid layer.

appropriate for the rapid granular flow regime, where particle interactions are characterized by short-duration collisional contacts. Such flows are usually driven by high rates of deformation.

Most theoretical analyses of granular flows are hindered by the complexity of conditions to be assumed at boundaries, either at the bounding walls or between two distinct phases within a flow. Unlike Newtonian flows, no-slip conditions are rarely encountered in most practical granular flows. Invariably, slip is present at the walls. The extent of slip depends on a variety of factors like particle and wall coefficients of restitution and friction, and the nature and size of asperities at the wall. The existence of slip, coupled with shearing of the flow at the wall, generates shear work, which may be converted into fluctuating kinetic energy of the individual particles. This energy is usually dissipated into pure heat either by inelastic collisions or by frictional interactions between particles and in interactions between particles and the bounding walls. Consequently, the bounding walls may serve as sources or sinks of fluctuating energy. As a result, the general flow field of a granular flow cannot be solved independently of the conditions at the boundaries. Variations of kinetic theory arguments have been used to balance momentum and energy generation, flux and dissipation for different boundary geometries and properties [10, 14–18].

While convective heat transfer to solid–gas flows is encountered in numerous process applications, studies of heat transfer in such media, both experimental and theoretical, have been relatively few in number. In such flows, while the effects of the interstitial fluid are neglected while studying the dynamical behavior of most granular flows, it plays a vital role in the heat transfer process. Sun and Chen [19] showed that in most cases, the heat transfer due to conduction at particle–particle and particle–wall contacts contributes negligibly to the overall heat transfer process unless the particles have very high conductivities and are placed in a vacuum. Hence, the dominant mode of heat transfer is through heat exchange between the particles and the interstitial fluid. Furthermore, in the case of spherical particles, the local solid fraction immediately adjacent to a wall is always zero, and all heat transfer from a heated wall is through the interstitial fluid. Schlunder [20] reviewed some of the earlier work in the area.

Sullivan and Sabersky [21] investigated the convective heat transfer from a flat plate immersed in a flowing granular medium in a vertical hopper-bin arrangement. They attempted to model the behavior of the fluid layer immediately adjacent to the heated surface in terms of a contact resistance that was directly proportional to the 'effective' thickness of the interstitial fluid layer adjacent to the wall and inversely proportional to the diameter of spherical particles in the granular medium. It was expected that the contact resistance should have the same numerical value for geometrically similar arrangements of particles adjacent to the wall. Conversely, any changes in the boundary conditions or particle sizes and shapes would alter the value of the contact resistance.

Spelt *et al.* [22], Patton *et al.* [23] and Ahn [24] extended Sullivan and Sabersky's work to investigate heat transfer to flows in an inclined chute at much higher velocities. They observed good agreement between their data and Sullivan and Sabersky's [21] theoretical model for slow high-density flows, but found that beyond a certain flow speed, the Nusselt number decreased with increasing Peclet numbers (or decreasing particle residence times adjacent to the wall). The reader is referred to Natarajan [25] or Natarajan and Hunt [26] for a more detailed discussion of the experimental work in inclined chute geometries.

There is little evidence, in published literature, of attempts at modeling the heat transfer phenomena in granular flows. Louge *et al.* [27] used kinetic theory developments to investigate heat transfer in dilute pneumatic systems transporting massive particles, while Boateng and Barr [28] developed a mathematical model to examine heat transfer in rotary kilns. Hsiau and Hunt [29] used kinetic-theory arguments to arrive at a steaming thermal conductivity value that was directly proportional to the square root of the granular temperature and varied inversely with the solid fraction of the material. Hunt [30] used a two-dimensional discrete-element computer simulation to determine the effective thermal conductivity and self-diffusivity for a bed of particles with random trajectories, but with no overall bed motion.

This work uses the constitutive relations based on dense gas kinetic theory developed by Lun *et al.* [6] to examine the heat transfer to granular flows from heated walls, in a vertical chute geometry. Comparisons are made with the experimental measurements of Sullivan and Sabersky [21] and Natarajan and Hunt [26]. The study also examines the effect of particle properties and boundary conditions on the density of the flow adjacent to the wall and on the resultant heat transfer rates.

ANALYTICAL BACKGROUND

This work examines the heat transfer in dense granular material flows in a two-dimensional, vertical channel, which is the geometry used in the experiments by Natarajan [25]. The constitutive model for granular flows, based on dense-gas kinetic theory (Lun *et al.* [6]) is utilized in order to establish the velocity, density and granular temperature fields in the vertical channel. The governing hydrodynamic equations for such granular flows are:

$$\frac{d\rho}{dt} = -\rho\nabla\cdot\mathbf{u} \tag{1}$$

$$\rho\frac{d\mathbf{u}}{dt} = \rho\mathbf{F} - \nabla\cdot\mathbf{P} \tag{2}$$

$$\frac{3}{2}\rho\frac{d\mathbf{T}}{dt} = -\mathbf{P}:\nabla\mathbf{u} - \nabla\cdot\mathbf{\Gamma} - \gamma \tag{3}$$

where ρ is the bulk flow density and is equal to the product of the particle density ρ_p and the solid fraction ν. In the above equation, $\mathbf{P}$ is the total stress tensor comprising of the contributions from the collisional and translational stress tensor components (Lun *et al.* [6]), $\mathbf{F}$ the specific body force, $\mathbf{\Gamma}$ the fluctuating energy flux and γ is the specific energy dissipated due to inelastic particle collisions. As explained in Lun *et al.* both $\mathbf{P}$ and $\mathbf{\Gamma}$ are composed of both the streaming and collisional components of momentum and energy transfer, respectively, The 'granular temperature', $\mathbf{T}$, is defined as the average of the sum of the squares of the three fluctuating velocity components and is a measure of the specific random kinetic energy of the flow.

Lun *et al.* [6] obtained the following expression for the stress tensor $\mathbf{P}$, the fluctuating energy flux $\mathbf{\Gamma}$ and the specific energy dissipation γ:

$$\mathbf{P} = \left[\rho_p g_1(\nu, e_p)\mathbf{T} - \rho_p\sigma\frac{8}{3\sqrt{\pi}}\eta\nu^2 g_0\mathbf{T}^{1/2}\nabla\cdot\mathbf{u}\right]\mathbf{I} - 2\rho_p\sigma g_2(\nu, e_p)\mathbf{T}^{1/2}\mathbf{S} \tag{4}$$

$$\mathbf{\Gamma} = -\rho_p\sigma[g_3(\nu, e_p)\mathbf{T}^{1/2}\nabla\mathbf{T} + g_4(\nu, e_p)\mathbf{T}^{3/2}\nabla\nu] \tag{5}$$

$$\gamma = \frac{\rho_p}{\sigma} g_5(\nu, e_p)\mathbf{T}^{3/2} \tag{6}$$

where $\mathbf{I}$ is the identity matrix and $\mathbf{S}$ is the deviatoric part of the rate of deformation tensor, and is given by:

$$\mathbf{S} = \tfrac{1}{2}(u_{n,p}+u_{p,n})-\tfrac{1}{3}u_{l,l}\delta_{n,p}, \quad l,n,p = x,y,z \tag{7}$$

and $\eta = \frac{1}{2}(1+e_p)$. Here ν is the solid fraction, σ the particle diameter and e_p the coefficient of restitution for collisions between particles.

Throughout this work, the form of the radial distribution function used is the one suggested for sheared flows [9]:

$$g_0(\nu) = (1-\nu/\nu^*)^{-2.5\nu^*}. \tag{8}$$

Here ν^* is the maximum shearable solid fraction for the particle assembly. It must be noted that the radial distribution function defined above is based on the assumption of collisional isotropy which requires an isotropic distribution of collision angles between the two colliding spheres.

The coefficients g_1, g_2, g_3, g_4 and g_5 are expressed as:

$$g_1(\nu, e_p) = \nu + 4\eta\nu^2 g_0 \tag{9}$$

$$g_2(\nu, e_p) = \frac{5\sqrt{\pi}}{96}\left\{\frac{1}{\eta(2-\eta)g_0} + \frac{8}{5}\frac{3\eta-1}{2-\eta}\nu + \frac{64}{25}\eta\left(\frac{3\eta-2}{2-\eta}+\frac{12}{\pi}\right)\nu^2 g_0\right\} \tag{10}$$

$$g_3(\nu, e_p) = \frac{25\sqrt{\pi}}{16\eta(41-33\eta)}\left\{\frac{1}{g_0} + \frac{12}{5}\eta[1+\eta(4\eta-3)]\nu + \frac{16}{25}\eta^2\left[9\eta(4\eta-3)+\frac{4}{\pi}(41-33\eta)\right]\nu^2 g_0\right\} \tag{11}$$

$$g_4(\nu, e_p) = \frac{15\sqrt{\pi}}{4}\frac{(2\eta-1)(\eta-1)}{41-33\eta}\left(\frac{1}{\nu g_0}+\frac{12}{5}\eta\right)\frac{d}{d\nu}(\nu^2 g_0) \tag{12}$$

$$g_5(\nu, e_p) = \frac{48}{\sqrt{\pi}}\eta(1-\eta)\nu^2 g_0. \tag{13}$$

Johnson and Jackson [17] derived boundary conditions for granular flows using arguments similar to those of Hui *et al.* [14], and also included frictional interactions. However, frictional interactions were not considered in this work as studies by Natarajan [25] indicated that the frictional model proposed by Johnson and Jackson [17] failed to predict physically plausible flow behavior in the limit of very high solid fractions. In the limiting case of purely collisional interactions between the wall and the flow particles, their conditions reduced to a form similar to that of Richman [15]. However, because their conditions did not invoke any explicit description of the boundary geometry, certain experimentally determined parameters have to be incorporated into their conditions. The boundary conditions derived by Johnson and Jackson [17] have been used in this work.

Equating the stress exerted by the flow on the boundary with the limit of the stress in the flowing material on approaching the boundary results in the following condition on the slip velocity,

$$\frac{\mathbf{u}_{sl}\cdot\mathbf{P}\cdot\mathbf{n}}{|\mathbf{u}_{sl}|} + \frac{\phi'\sqrt{3}\pi\rho_p\nu\mathbf{T}^{1/2}|\mathbf{u}_{sl}|g_0(\nu)}{6\nu^*} = 0. \tag{14}$$

The slip velocity, $\mathbf{u}_{sl} = \mathbf{u}-\mathbf{u}_{wall}$, is the relative velocity between the particles in contact with the wall and the wall itself. The unit normal vector directed inwards from the wall into the flow is designated as $\mathbf{n}$. The first term in equation (14) above is the limit of the stress in the flow approaching the wall. The second term represents the stress acting on the boundary due to particle–wall collisions. The 'specularity coefficient' ϕ' is defined as the average fraction of the relative tangential momentum transferred during a collision between the particle and the boundary. It serves as a measure of the roughness and orientation of the bounding surface and ranges from zero for perfectly specular collisions to unity for perfectly diffuse collisions.

A boundary condition on the fluctuating energy is obtained from an energy balance on a slice of vanishingly small thickness of material enclosing an element of the solid boundary and is given by:

$$-\mathbf{n}\cdot\boldsymbol{\Gamma} = \frac{\pi\rho_p\nu(1-e_w^2)\sqrt{3}\mathbf{T}^{3/2}g_0(\nu)}{\nu^*} - \frac{\phi'\sqrt{3}\pi\rho_p\nu\mathbf{T}^{1/2}|\mathbf{u}_{sl}|^2 g_0(\nu)}{6\nu^*}. \tag{15}$$

While the first term on the right hand side of equation (15) represents the dissipation of fluctuation energy due to inelastic particle–wall collisions, the second term represents the production of fluctuation energy at the boundary due to shear work. The left hand side of equation (15) represents the net fluctuation energy flux into the bulk. It is important to note that implicit in equation (15) is the assumption that all shear work due to collisional stresses is converted into random fluctuation energy and not into heat.

The temperature distribution across the flow field was determined by solving the following internal energy equation over the flow field.

$$\rho c_p\frac{DT}{Dt} = -\nabla\cdot q_h + \gamma \tag{16}$$

where T refers to the thermodynamic temperature and γ is the contribution due to the inelastic dissipation of random kinetic energy into pure thermal energy. The relation $\nu\rho_p c_p+(1-\nu)\rho_{air}c_{air} \approx \rho c_p$ was applied in the above equation. Here, ρ_p and c_p are the density and specific heat capacity for the particles and ρ_{air} and c_{air} are the corresponding qualities for the air. Further-

more, the diffusive flux term in equation (16) may be written as:

$$\nabla \cdot q_h = -\nabla \cdot (k_{tot} \nabla T) \tag{17}$$

where k_{tot} is defined as the simple sum of the thermal conductivity contributions due to molecular conductivity, k_{mc} and the streaming or kinetic conductivity, k_{kt}, arising out of the kinetic theory analysis.

Gelperin and Einstein [31] proposed the following expression for the effective molecular conductivity, k_{mc} of a solid–gas bulk material,

$$\frac{k_{mc}}{k_g} = 1 + \frac{\nu\left(1 - \frac{k_g}{k_s}\right)}{\frac{k_g}{k_s} + 0.28(1-\nu)^{0.63\left(\frac{k_g}{k_s}\right)^{-0.18}}} \tag{18}$$

where k_g and k_s are the conductivities of the gas and the solid material, respectively.

Hsiau and Hunt [29] used arguments based on the dense-gas kinetic theory model, assuming that the only mode of heat transfer was the streaming mode. Heat transfer during the collisional interactions amongst the particles was assumed to be negligible. Apart from the assumptions inherent in the kinetic theory analysis, the Biot number was assumed to be less than 0.1 to allow a lumped mass analysis for the particles. Under these assumptions, they arrived at the following expression for the effective conductivity k_{kt}:

$$k_{kt} = \frac{\rho c_p \sigma \left(\frac{T}{\pi}\right)^{1/2}}{9\nu g_0(\nu)}. \tag{19}$$

Equation (19) implies that a decrease in the solid fraction would allow particles to stream across larger distances, thereby enhancing the effective conductivity.

A comparison of equations (18) and (19) suggests that for low-density, highly sheared flows, the two mechanisms may be operating in opposition to one another. A decrease in density reduces the bulk molecular conductivity, but may simultaneously enhance the streaming conductivity.

The first part of the next section describes the numerical solution of the momentum and fluctuation energy equations [equations (2) and (3)] leading to the determination of mean and fluctuation velocity profiles for granular flows in a vertical chute. Comparisons are made with experimentally measured profiles [32]. The second part presents the results obtained by the numerical solution of the internal energy equation [equation (16)]. Convective heat transfer coefficients were evaluated for a range of flow situations and compared with experimental data [26].

MOMENTUM AND FLUCTUATION ENERGY EQUATIONS

For the numerical solutions, the flow in a vertical channel is assumed to be steady and two-dimensional, with fully developed density, velocity and fluctuation velocity profiles. The x-direction was the direction of mean motion while the y-direction was transverse to the direction of mean flow of the material. For the two-dimensional flow, the equations (2) and (3) reduce to:

$$-\left(\frac{\partial P_{xx}}{\partial x} + \frac{\partial P_{xy}}{\partial y}\right) + \rho g = 0 \tag{20}$$

$$\left(\frac{\partial P_{yy}}{\partial y}\right) = 0 \tag{21}$$

and

$$-P_{xy}\frac{\partial u_x}{\partial y} - \frac{\partial \Gamma_y}{\partial y} - \gamma = 0. \tag{22}$$

The contribution to the normal stresses from the kinetic-theory model [equation (4)] is given by:

$$P_{xx} = P_{yy} = \rho_p g_1(\nu, e_p)\mathbf{T} \tag{23}$$

and the shear stresses are given by:

$$P_{xy} = P_{yx} = -\rho_p \sigma g_2(\nu, e_p)\mathbf{T}^{1/2}\frac{du_x}{dy}. \tag{24}$$

The flux of fluctuating energy in the direction normal to the walls is

$$\Gamma_y = -\rho_p \sigma \left[g_3(\nu, e_p)\mathbf{T}^{1/2}\frac{d\mathbf{T}}{dy} + g_4(\nu, e_p)\mathbf{T}^{3/2}\frac{d\nu}{dy}\right]. \tag{25}$$

Hsiau [33] showed that, for a fully developed flow, $\partial P_{xx}/\partial x$ is negligible for a vertical distance greater than twice the channel depth.

The non-dimensional momentum equations are obtained by substituting the expressions for the stresses from equations (24)–(26) into equations (20)–(22) and by substituting for the non-dimensional variables. As a result, the following expressions are obtained,

$$\frac{d}{dY}\left[g_2(\nu, e_p)\mathbf{T}^{*1/2}\frac{du_x^*}{dY}\right] + A^{3/2}\nu = 0 \tag{26}$$

and

$$\frac{d}{dY}[g_1(\nu, e_p)\mathbf{T}^*] = 0. \tag{27}$$

The non-dimensionalized form of the fluctuation energy equation is given by:

$$\frac{d}{dY}\left[g_3(\nu, e_p)\mathbf{T}^{*1/2}\frac{d\mathbf{T}^*}{dY} + g_4(\nu, e_p)\mathbf{T}^{*3/2}\frac{d\nu}{dY}\right]$$

$$+ Ag_2(\nu, e_p)\mathbf{T}^{*1/2}\left(\frac{du_x^*}{dY}\right)^2 - A^2 g_5(\nu, e_p)\mathbf{T}^{*3/2} = 0 \tag{28}$$

with non-dimensional variables

$$X = \frac{x}{\sigma}$$

$$Y = \frac{y}{W}$$

$$u_x^* = \frac{u_x}{\sqrt{gW}}$$

$$P_{xx}^* = \frac{P_{xx}}{\rho_p g \sigma}$$

$$\mathbf{T}^* = \frac{\mathbf{T}}{g\sigma}$$

$$A = \frac{W}{\sigma}$$

where W is the half-width of the channel and g is the acceleration due to gravity.

The nondimensionalized form of the boundary conditions (Johnson and Jackson [17]) from equations (14) and (15) for the shear stress and the balance of fluctuation energy at the wall, respectively, are given by:

$$-g_2(\nu, e_p)A^{-1/2}\mathbf{T}^{*1/2}\frac{du_x^*}{dY} = \frac{\phi'\sqrt{3}\pi\nu A^{1/2}\mathbf{T}^{*1/2}|u_{sl}^*|g_0(\nu)}{6\nu^*} \tag{29}$$

and

$$-\left[g_3(\nu, e_p)\frac{d\mathbf{T}^*}{dY} + g_4(\nu, e_p)\mathbf{T}^*\frac{d\nu}{dY}\right] = -\frac{\phi'\sqrt{3}\pi\nu A^2 u_{sl}^{*2} g_0(\nu)}{6\nu^*} + \frac{\pi\nu(1-e_w^2)\sqrt{3}\mathbf{T}^* g_0(\nu)}{4\nu^*}. \tag{30}$$

An investigation of equation (27) shows that given a constant particle coefficient of restitution e_p, the solid fraction at any point is a function of only the normalized granular temperature $\mathbf{T}^*$. Therefore, all functions of ν can be written in terms of the granular temperature in equations (26) and (28). Consequently, a system of two coupled, ordinary second-order differential equations for the normalized flow velocity, u_x^*, and normalized granular temperature $\mathbf{T}^*$ has to be solved.

These equations were solved using a fourth-order Runge–Kutta scheme. Given the two second-order equations, a total of four boundary conditions are required to solve the problem. Two of these conditions are obtained from equations (29) and (30) for the shear stress and fluctuation energy balance at the wall. The other two boundary conditions are obtained by using the symmetry of the channel to set du_x^*/dY and $d\mathbf{T}^*/dY$ equal to zero at the channel center-line $Y = 0$. A 'shooting' method was used to solve the resultant boundary value problem. Values for u_x^* and $\mathbf{T}^*$ were guessed for a particular value of solid fraction at the center-line and the equations were integrated from the center-line to the wall. The process was iterated, using a globally convergent Newton–Raphsons scheme to match the boundary conditions at the wall. Convergence was assumed to have been achieved when the difference between the left and right hand sides of equations (29) and (30) was less than 1×10^{-6}.

From equations (26) and (28), as well as the boundary conditions (equations 29 and 30), several physical parameters need to be specified. In the literature, little information deals with actual measurements of these parameters. The coefficient of restitution for particle–particle collisions, e_p, was assumed to be 0.95 [34], unless otherwise specified. A value of 0.65 was assumed for the maximum shearable solid fraction ν^* [17]. Since no measurements of specularity coefficients ϕ' are available, reasonable values had to be assumed arbitrarily. Unless specified otherwise, a value of $\phi' = 0.85$ was chosen for all the numerical calculations simulating rough walls. This value was chosen on the basis of the comparisons between theoretical and experimental streamwise velocity profiles, and is representative of a wall that is very rough. Johnson *et al.* [35] assumed values of $\phi' = 0.25$ for aluminum walls and $\phi' = 0.6$ for 160 grit sandpaper. In the current study, walls with glass particles glued to them are assumed to be rougher than those examined by Johnson *et al.* [35]. A range of values were considered for the particle–wall coefficient of restitution e_w.

RESULTS

The effect of varying the wall–particle coefficient of restitution (e_w) is presented in Figs. 1–3. While the dense-gas kinetic theory model of Lun *et al.* [6] is based on the assumption that the value of e_p is very close to one, there is no such stipulation for e_w, which appears only in the boundary conditions. Figure 1 shows the mean velocity profiles, for different values of the centerline solid fraction, for values of e_w equal to 0.95, 0.50 and 0.20. For moderate or highly dense flows, as shown in Fig. 1, there is a distinct central uniform velocity regime and a sheared regime adjacent to the walls. The granular temperature profiles, shown in Fig. 2 increase from the center towards the walls. The solid fraction profiles in Fig. 3 depict maximum values at the center and more dilated regions adjacent to the walls. While profiles have been presented for centerline solid fractions of 0.36 and less, it must be cautioned that these are primarily of academic interest only. At such low density values, particle interactions in the vertical chute are likely to be negligible, with each particle in a state of free fall under the influence of gravity. While the velocity profiles remain similar in shape and magnitude, comparisons of the temperature and density profiles for the three values of e_w show interesting changes. A lower value of e_w implies greater dissipation of random energy at the wall. Hence for the cases of $e_w = 0.50$ and $e_w = 0.20$, the granular temperatures decrease adjacent to the wall,

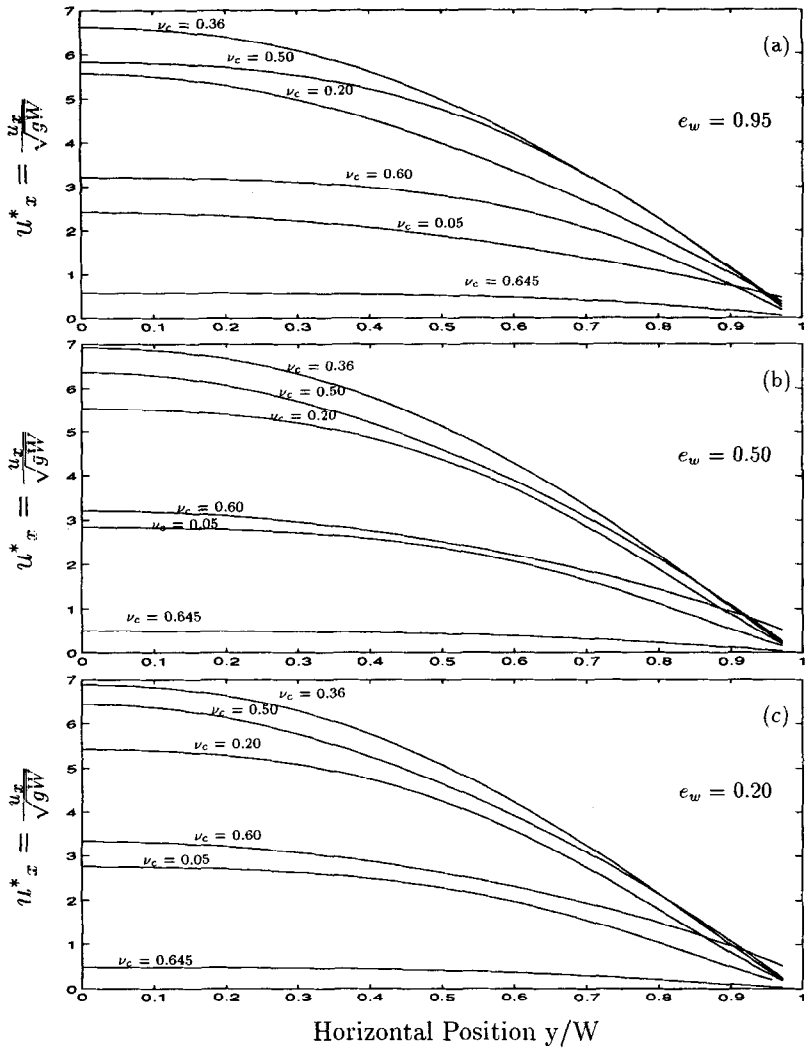

Fig. 1. Comparison of the theoretical nondimensionalized streamwise mean velocity profiles, for values of (a) $e_w = 0.95$, (b) $e_w = 0.50$ and (c) $e_w = 0.20$. ν_c is the centerline solid fraction. $e_p = 0.95$. $W = 3.5$ cm.

accompanied by increased solid fractions in the same region. Reduced granular temperatures cause greater 'clumping' of particles. Qualitatively similar behavior is observed in experimentally measured transverse fluctuation velocity profiles [32]. As discussed earlier, frictional interactions at the wall could also be responsible for such a lowering of fluctuation velocities close to the walls. All the above calculations are for $\phi' = 0.85$.

Comparisons between calculated and measured mean streamwise velocity profiles are presented in Fig. 4. The figures compare the numerically calculated mean velocity profiles (for a combination of $e_p = e_w = 0.85$) with experimental data [25, 32]. The agreement between the numerical and experimental mean velocity profiles is good for the sheared regimes. A comparison of the graphs of the numerically computed profiles of $\mathbf{T}^{1/2}$ with the measured profiles of the transverse fluctuation velocities [25] is depicted in Fig. 5. The numerical solutions overpredict the fluctuation velocities in the sheared regimes adjacent to the wall, but underpredict these values in the regimes away from the wall. Also, the gradients in the fluctuation velocity are more significant in the numerical solutions. It must be noted that the kinetic theory model applied in this work assumes the fluctuation velocities to be isotropic. Experimental studies by Natarajan *et al.* [32] and Drake [36] indicated that fluctuation velocities were strongly anisotropic. Also, the numerical solutions predicted solid fraction in the range of 0.63–0.65 across the flow section for the case compared here. In contrast, Natarajan [25] observed distinct low density sheared regimes adjacent to the wall. More detailed comparisons between numerical and experimental data are found in Natarajan [25].

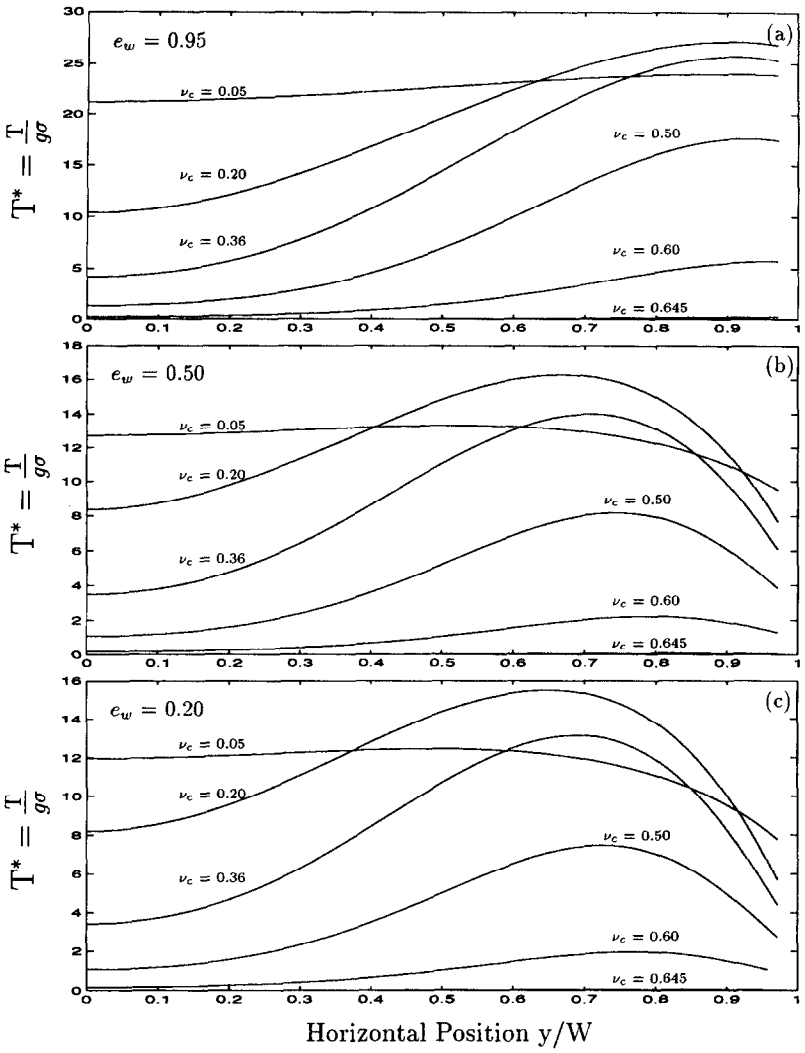

Fig. 2. Comparison of the theoretical nondimensionalized granular temperature profiles, for values of (a) $e_w = 0.95$, (b) $e_w = 0.50$ and (c) $e_w = 0.20$. ν_c is the centerline solid fraction. $e_p = 0.95$. $W = 3.5$ cm.

INTERNAL ENERGY EQUATION

The internal energy equation [equation (16)] was solved numerically for the entire flow field to determine the average heat transfer coefficients. In the regime immediately adjacent to the wall, where solid fractions become extremely low, the approximation $\nu\rho_p c_p + (1-\nu)\rho_{air}c_{air} \approx \rho c_p$ was replaced by the complete, unapproximated expression, to account for the increased influence of the interstitial fluid. A power-law scheme [37, 38] was used to discretize the temperature field.

To solve for the temperature field, the momentum equations were first solved to establish the mean streamwise velocity, granular temperature and solid fraction profiles. As discussed earlier, the effect of the interstitial fluid can be neglected when investigating the dynamics of the system, but cannot be neglected in the heat transfer problem. The interstitial fluid, especially the layer adjacent to the heated wall plays a crucial role in the heat transfer process. For spherical particles, the solid fraction goes to zero at a flat bounding wall. However, as evident from the solid fraction profiles examined previously, the kinetic theory solutions always predict significant, non-zero solid fractions at the wall, as a result of the 'continuum' assumption. Hence, in order to generate realistic solutions to the heat transfer problem, assumptions are needed about the solid fraction profile adjacent to the wall. More specifically, a profile form has to be assumed such that the solid fraction decreases from the value predicted by the kinetic-theory model at a distance of half a particle diameter from the wall to a value of zero at the wall. Using a simple analysis,

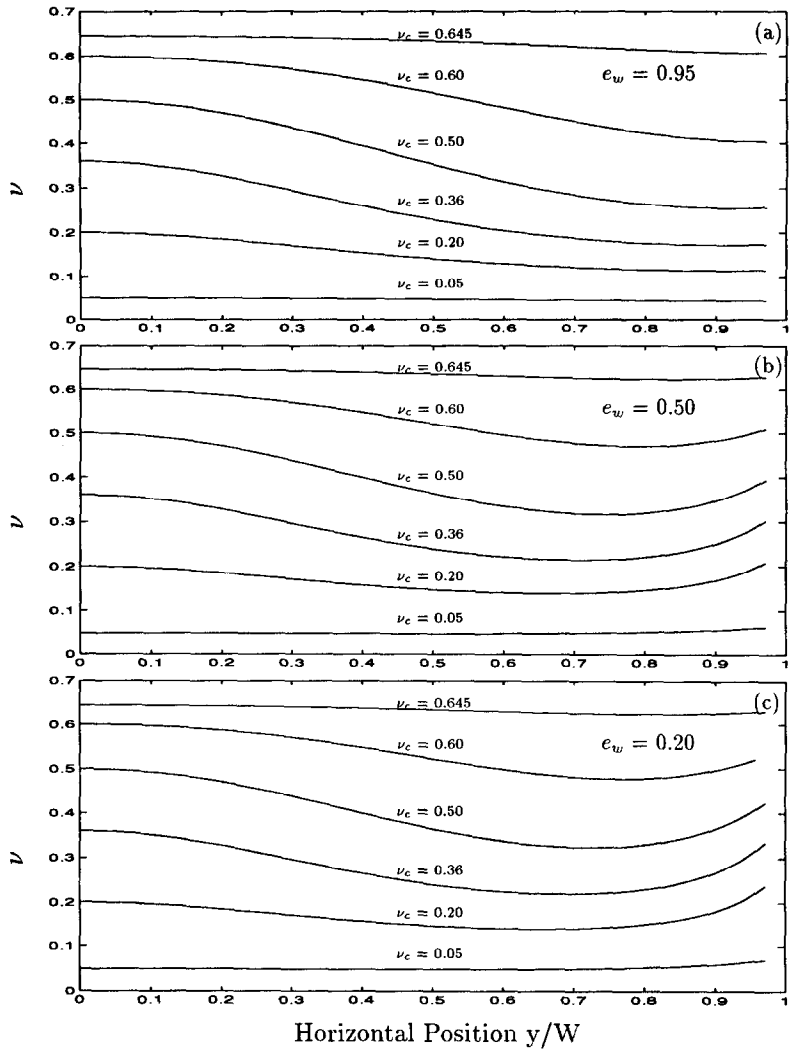

Fig. 3. Comparisons of the theoretical solid fraction profiles, for values of (a) $e_w = 0.95$, (b) $e_w = 0.50$ and (c) $e_w = 0.20$. ν_c is the centerline solid fraction. $e_p = 0.95$. $W = 3.5$ cm.

based on Fig. 6, the solid fraction profile adjacent to the wall was assumed to be of the form:

$$\nu(y) = \nu_{\sigma/2}\left(1-\left(\frac{y-(W-\sigma/2)}{\sigma/2}\right)^2\right) \tag{31}$$

where $\nu_{\sigma/2}$ is the solid fraction at a distance of half a particle diameter from the wall. Also, though there is a slip between the glass particles and the wall, it is realistic to expect that a no-slip condition would exist between the air and the wall. Hence, the air velocity was assumed to be linearly decreasing to zero over the distance of half a particle diameter adjacent to the wall, by adopting the profile:

$$u_x(y) = u_{x-\sigma/2}\left(1-\frac{y-(W-\sigma/2)}{\sigma/2}\right). \tag{32}$$

Furthermore, in order to be consistent with the assumed solid fraction profile adjacent to the wall, the granular temperature was also assumed to go to zero at the wall. This was done to account for the fact that it is ambiguous to have a non-zero granular temperature at a position where the solid fraction is zero. Therefore, when evaluating the value of k_{kt} in the regime within half a particle diameter from the wall, a linear profile was assumed for the square root of the granular temperature, of the form:

$$\mathbf{T}^{1/2}(y) = \mathbf{T}_{\sigma/2}^{1/2}\left(1-\frac{y-(W-\sigma/2)}{\sigma/2}\right) \tag{33}$$

where $\mathbf{T}_{\sigma/2}$ is the value of the granular temperature at a distance of half a particle diameter from the wall. Such an assumption is unrealistic to a certain degree, as ideally, particles impacting the wall have a non-zero translational fluctuation velocity that is constant for the whole particle. However, immediately adjacent to the wall, the continuum assumption governing the

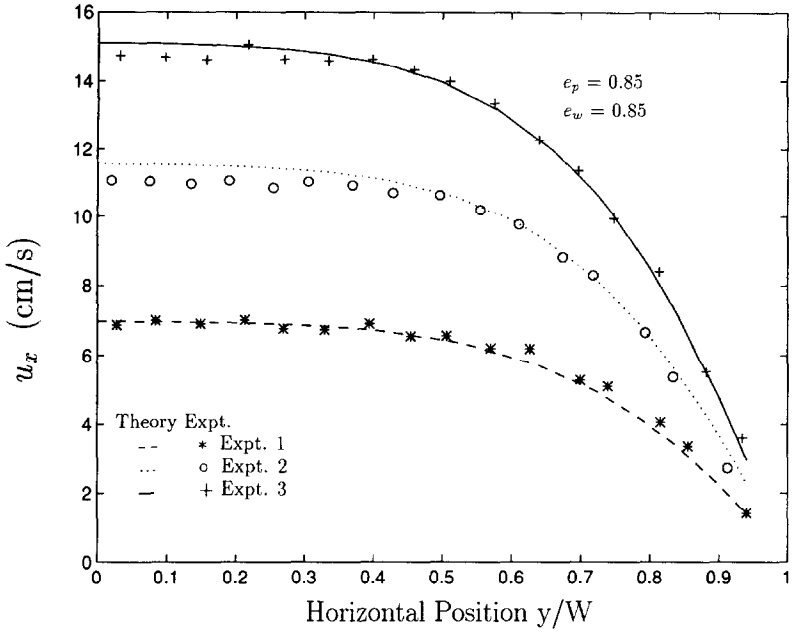

Fig. 4. Comparison of experimental and theoretical mean streamwise velocity profiles. $e_p = 0.85$. $e_w = 0.85$. $W = 2.5$ cm.

kinetic theory solutions breaks down as changes in solid fraction profiles occur over distances much less than a particle diameter. This is contrary to the stipulation of the continuum assumption that flow properties remain constant over a distance of several particle diameters. However, it is evident from the experimental data that steep gradients in the transverse fluctuation velocity profile occur over distances less than a particle diameter, in the sheared regimes adjacent to the wall. Physical property values used in the numerical solutions are listed in Table 1. The temperature at the inlet section, as well as at the centerline was assumed to be 24°C.

RESULTS

To make comparisons with experimental data and the Sullivan–Sabersky model, a series of plug flow solutions were generated, using the kinetic theory model without friction, by assuming a value of 0.01 for the specularity coefficient ϕ'. The values of the mean solid fractions for all the flows in this set of numerical solutions were in the range 0.64–0.65. While this regime is certainly not a rapid granular flow regime and hence cannot be described by a kinetic theory model, the purpose of the exercise was to generate a set of plug flows, with uniform velocity and solid fraction profiles, using the numerical scheme already in place.

On the basis of their observations and experimental results, Sullivan and Sabersky [21] arrived at the following semi-empirical relation:

$$Nu^* = \frac{1}{\left(\chi + \frac{1}{2}\sqrt{\frac{\pi}{Pe^*}}\right)} \tag{34}$$

where

$$Nu^* = \frac{h\sigma}{k_g} \tag{35}$$

and

$$Pe^* = \left(\frac{UL}{\alpha_c}\right)\left(\frac{\sigma}{L}\right)^2\left(\frac{k_c}{k_g}\right)^2. \tag{36}$$

The expression in equation (34) was derived for a uniform plug flow, at a velocity U past a heated plate of length L. The thermal conductivity and the diffusivity of the bulk material, at critical density, are given by k_c and α_c, respectively, while k_g is the conductivity of the interstitial fluid. The length-averaged heat transfer coefficient is given by h. In essence, this model considered the flow regime to be composed of two distinct regions: the bulk flow material, considered as a continuum with uniform density (the critical density) and velocity, and an interstitial fluid layer separating the heated wall from the granular material continuum. The interstitial fluid layer was assumed to have a thermal resistance χ, which may be defined as $\chi^{-1} = (h_{wp}\sigma/k_g)$ where h_{wp} is the wall–particle heat transfer coefficient (or the thermal conductance between particles and the wall). The thermal conductance is expected to be a strong function of the local geometric arrangement of particles as this would

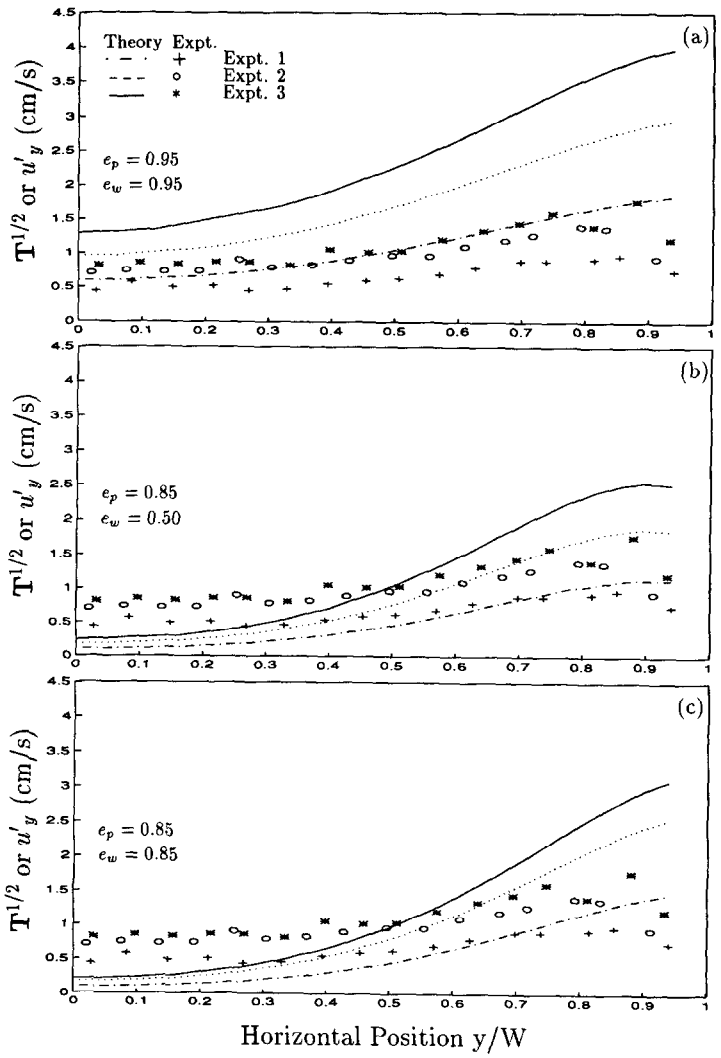

Fig. 5. Comparisons of theoretical root mean square fluctuation velocity profiles with experimental transverse fluctuation velocity profiles for values of (a) $e_p = 0.95$, $e_w = 0.95$, (b) $e_p = 0.85$, $e_w = 0.50$, and (c) $e_w = 0.85$, $e_w = 0.85$. $W = 2.5$ cm.

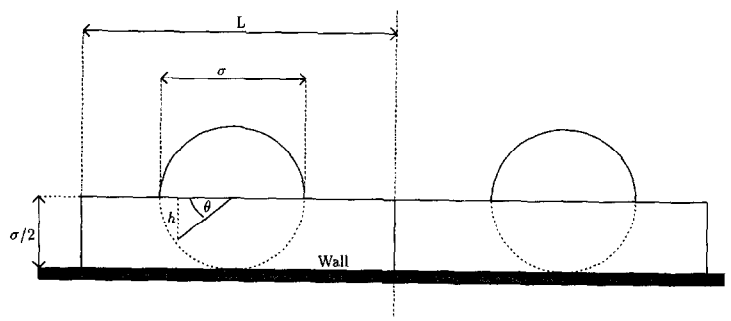

$$\nu_{\sigma/2} = \frac{\pi\sigma}{4L}$$

At a distance h from the particle centerline, the solid fraction is given by

$$\nu = \frac{\pi(\sigma/2)^2}{2L(\sigma/2)}\cos\theta \quad = \nu_{\sigma/2}\left(1 - \left(\frac{h}{\sigma/2}^2\right)\right)$$

Fig. 6. Schematic for the assumed functional form of the solid fraction near the wall.

Table 1. Property values used in the numerical calculations

ρ_p	2500 kg m^{-3}
c_p	903.95 J kg °C^{-1}
c_{air}	1005.70 J kg °C − 1
k_g	0.026 W m °C^{-1}
k_s	0.910 W m °C^{-1}
k_c	0.210 W m °C^{-1}
α_c	1.5×10^{-7} m^2 s^{-1}

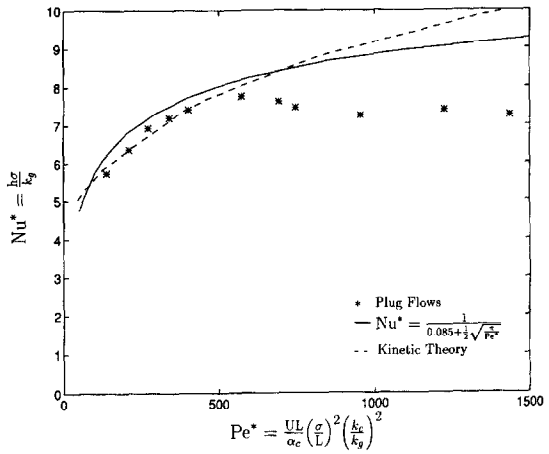

Fig. 7. Variation of Nu^* and Pe^*. Comparison of the measured data for plug flows (Natarajan and Hunt [26]) with the semi-empirical Sullivan and Sabersky relation and the numerical calculations based on kinetic theory. $\sigma = 3$ mm. $e_p = 0.95$, $e_w = 0.50$ and $\phi' = 0.025$ for the kinetic theory solution.

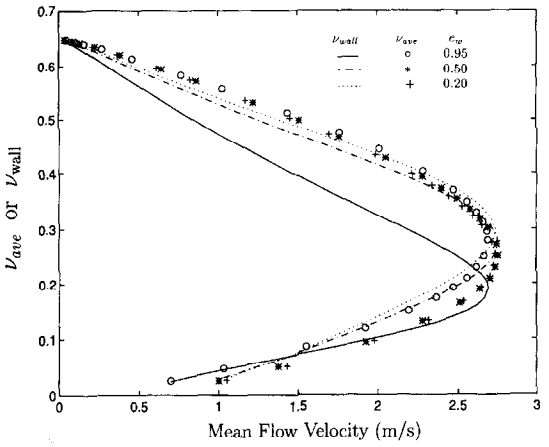

Fig. 8. Variation of the theoretical mean solid fraction (ν_{ave}) and the solid fraction at the wall (ν_{wall}) with the mean flow velocity. $e_p = 0.95$. Note that both symbols and lines in the figure represent numerically calculated values and do not represent experimental data.

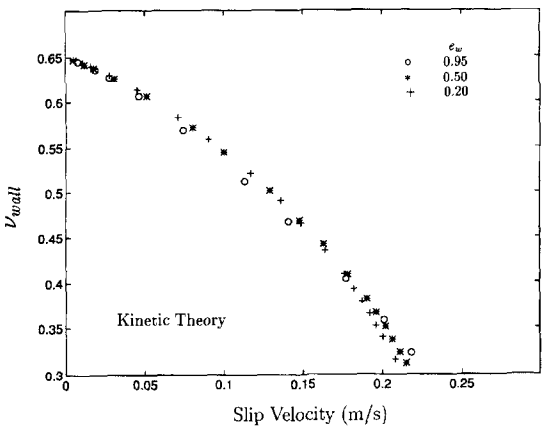

Fig. 9. Variation of the theoretical solid fraction at the wall (ν_{wall}) with the flow slip velocity. $e_p = 0.95$. Note that the symbols in the figure represent numerically calculated values and do not represent experimental data.

significantly influence the 'effective' thickness of the interstitial fluid layer. As a consequence, χ would depend on factors like the particle shape and the wall surface roughness.

Sullivan and Sabersky [21] found good agreement between their measurements and their theoretical model. However, their experiments were performed in the plug flow regime with negligible variations in flow densities adjacent to the heated plate.

Figure 7 compared the variation of Nu^* with Pe^* for the experimental data from Natarajan and Hunt [32] and the Sullivan–Sabersky semi-empirical model with the calculations for the plug flows generated from kinetic-theory. Up to a value of $Pe^* = 600$ there is a good agreement among the three different sets. However, neither the Sullivan–Sabersky model nor the calculations based on kinetic theory can replicate the measured plateau of the heat transfer coefficients at higher values of Pe^*. Both the Sullivan–Sabersky and kinetic-theory results are based on assumptions of constant flow density, contrary to the observations in the actual experiments.

To investigate the convective heat transfer behavior in sheared flows, three combinations of e_p and e_w were chosen to integrate the momentum equations for a range of centerline solid fraction values from 0.05–0.6495. The value of e_p was kept constant at 0.95 while the values of e_w were set at 0.2, 0.5 and 0.95 for the three sets. All the solutions were for a value of $\phi' = 0.85$. As discussed earlier, the density of the flows adjacent to the walls, plays an important role in determining the heat transfer coefficients, especially for flows that are subjected to high shear. Figure 8 shows the variation of the average solid fraction (ν_{ave}) and ν_{wall} (or $\nu_{\sigma/2}$), with the average velocity. It is observed that for $e_w = 0.95$, the difference between the values for ν_{ave} and ν_{wall} is quite significant. However, this difference decreases with a decrease in the value of e_w. The variation of ν_{wall} with the slip velocity is shown in Fig. 9. For the regime of solutions physically plausible for flows in a vertical channel ($\nu > 0.3$), both ν_{ave} and ν_{wall} decrease with an increase in velocity, qualitatively the same behavior as that observed in experiments by

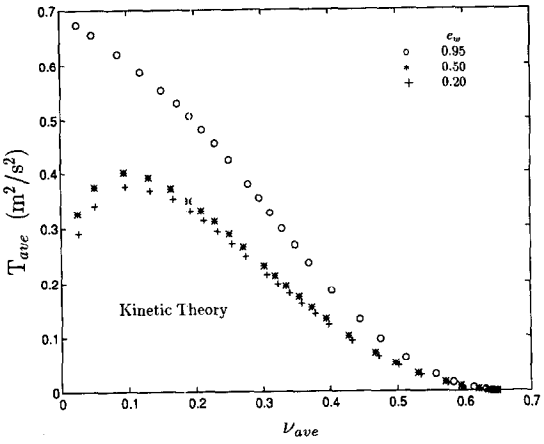

Fig. 10. Variation of the theoretical average granular temperature with the average solid fraction (ν_{ave}). $e_p = 0.95$. Note that the symbols in the figure represent numerically calculated values and do not represent experimental data.

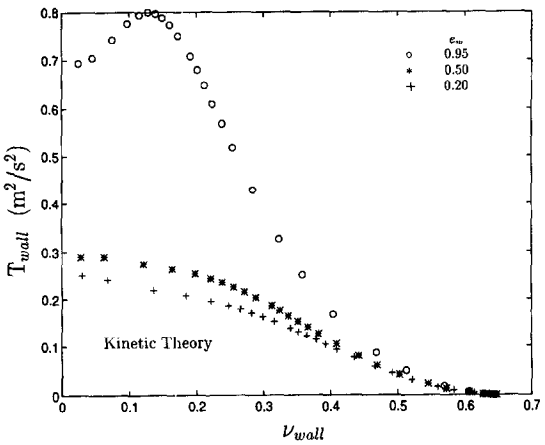

Fig. 11. Variation of the theoretical wall granular temperature with the wall solid fraction (ν_{wall}). $e_p = 0.95$. Note that the symbols in the figure represent numerically calculated values and do not represent experimental data.

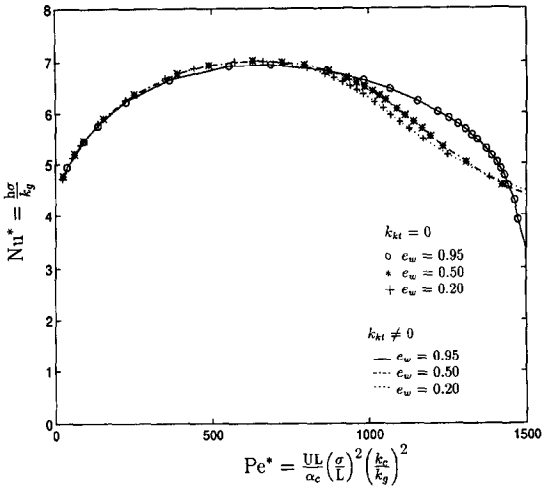

Fig. 12. Variation of Nu^* and Pe^*. Comparison of the theoretical solutions with, and without, the influence of the kinetic conductivity (k_{kt}) contribution. $\sigma = 3$ mm. $e_p = 0.95$. Note that both the symbols and lines in the figure represent numerically calculated results and do not represent experimental data.

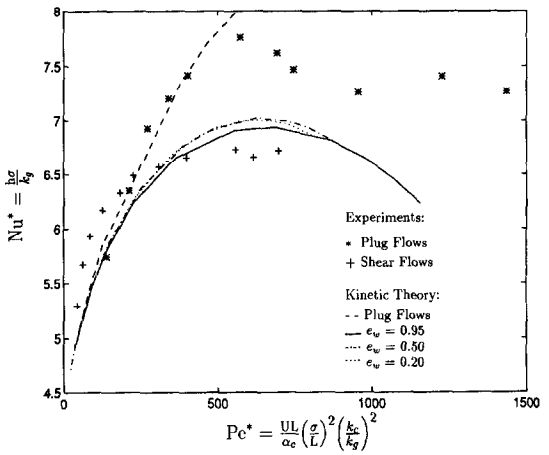

Fig. 13. Variation of Nu^* and Pe^*. Comparison of the experimentally measured data for plug and shear flows (Natarajan and Hunt [26]) with numerically calculated results. $\sigma = 3$ mm. $e_p = 0.95$.

Patton *et al.* [23] and Ahn [24]. It is noteworthy that, for values of $\nu > 0.3$, a change in the value of e_w does not influence these curves significantly. Another detail is the difference between the values of ν_{ave} and $\nu_{\sigma/2}$ in a flow. These results suggest that the average solid fraction may not be the appropriate parameter to use when evaluating thermal properties for the particle–air mixture adjacent to the wall.

The variation of the average granular temperature with the average solid fraction is presented in Fig. 10, while Fig. 11 depicts the corresponding values at the wall. The granular temperature decreases with an increase in solid fraction, except at extremely low solid fractions.

The results of the heat transfer calculations for the sheared flows are shown in Fig. 12 in the form of a graph of Nu^* vs. Pe^*. The lines depict the results obtained by suppressing the contribution of k_{kt} towards the net conductivity while the symbols depict the results obtained by including k_{kt}. For particles of 3 mm diameter, the kinetic contribution is negligible over the whole range of solid fractions and shear rates. A comparison of the numerical results with the experimental data for both sheared and plug flows [26] is presented in Fig. 13. The numerically calculated profiles for the sheared flows show a maximum value for Nu^*, similar to the experimental results of Spelt *et al.* [22], Patton *et al.* [23] and Ahn [24]. However, a comparison of the numerical profiles with the experimental data for sheared flows shows the kinetic theory underpredicting heat transfer coefficients for values of $Pe^* < 300$. Also, the theoretical results do

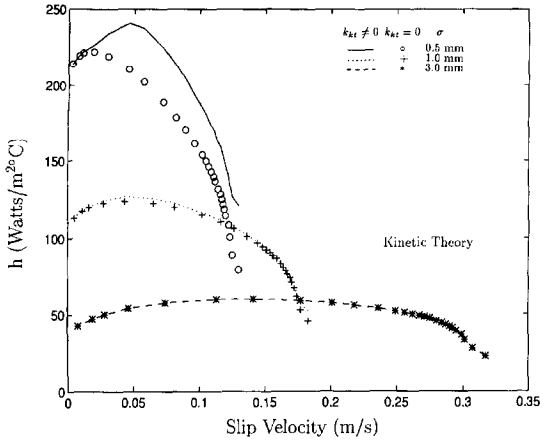

Fig. 14. Variation of the heat transfer coefficient with flow slip velocity. Comparison of the influence of particle diameter on the heat transfer coefficient. $e_p = 0.95$. Note that both the symbols in lines in the figure represent numerically calculated results and do not represent experimental data.

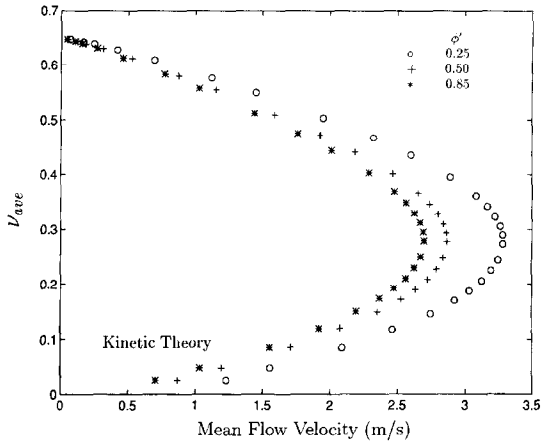

Fig. 15. The effect of varying the value of the specularity coefficient ϕ' on the variation of the average solid fraction (ν_{ave}) with the mean flow velocity. $e_p = 0.95$, $e_w = 0.50$. Note that the symbols in the figure represent numerically calculated results and do not represent experimental data.

not predict the plateau of the heat transfer coefficients observed in the experiments for higher velocities.

To examine the influence of particle size on the contribution of k_{kt} towards the effective heat transfer, solutions were also generated for particle diameters of 1 mm and 0.5 mm (with the size of the channel scaled so that W/σ was constant for all three cases) with $e_p = e_w = 0.95$. The length of the heated plate was set at 82.16 cm for each value of the particle diameter. The values of the average heat transfer coefficient h vs. the slip velocity are plotted in Fig. 14. The influence of k_{kt} increases with a decrease in the particle diameter. In the case of the smallest particle size investigated (0.5 mm), the maximum value of the heat transfer coefficient is achieved at a slip velocity three times greater in the case where the streaming component is included, than in the case where it is not. The value of the peak is also higher for the case including the effect of k_{kt}. Smaller particle diameters were not investigated as it was expected that at such sizes the assumption neglecting the effect of the interstitial fluid while determining the flow dynamics would no longer be valid.

All the results described previously were for a specularity of 0.85. Figures 15–18 investigate the effect of varying the value of ϕ'. From the figures, it is apparent that the effect of lowering the value of ϕ' is to cause greater 'clumping' of particles, increasing the solid fraction close to the walls. Consequently, as evident from Fig. 18, the value of Nu^* increases with a decrease in the value of ϕ' for a given value of Pe^*. As elucidated by the discussion about plug flows earlier in this section, a lower value of the specularity coefficient leads to less shearing at the wall thereby leading to higher solid fractions.

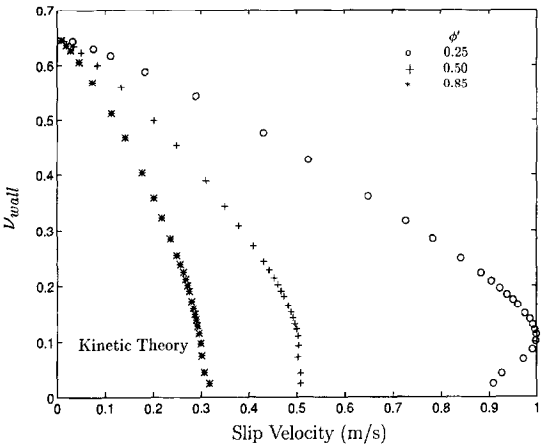

Fig. 16. The effect of varying the value of the specularity coefficient ϕ' on the variation of the wall solid fraction (ν_{wall}) with the flow slip velocity. $e_p = 0.95$, $e_w = 0.50$, $\sigma = 3$ mm. Note that the symbols in the figure represent numerically calculated results and do not represent experimental data.

CONCLUSIONS

Theoretical solutions, based on a dense-gas kinetic theory model, were generated to study and compare experimental and theoretical results for velocity profiles and heat transfer characteristics in granular flows in a vertical chute. Calculated mean velocity profiles were found to be in good agreement with experimental data. The theoretical solutions, in these cases, predicted solid fractions in the range of 0.64–0.65 across the entire flow section. However, in the actual experiments, there were distinct sheared regimes where the solid fractions were lower than the close-packed value. Also, the theoretical profiles for the granular temperature showed a much stronger dependence on the shear rate than was evident in the experimental data. Furthermore, because of the assumptions of isotropy in the granular temperature, the kinetic theory results were unable to replicate the anisotropic distribution of the fluctuation velocities observed experimentally.

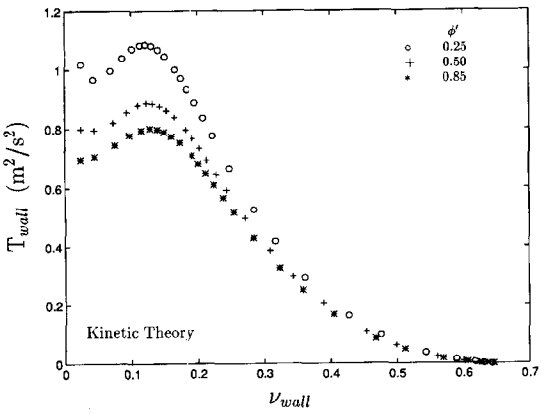

Fig. 17. The effect of varying the value of the specularity coefficient ϕ' on the variation of the wall granular temperature with wall solid fraction (ν_{wall}). $e_p = 0.95$, $e_w = 0.50$, $\sigma = 3$ mm. Note that the symbols in the figure represent numerically calculated results and do not represent experimental data.

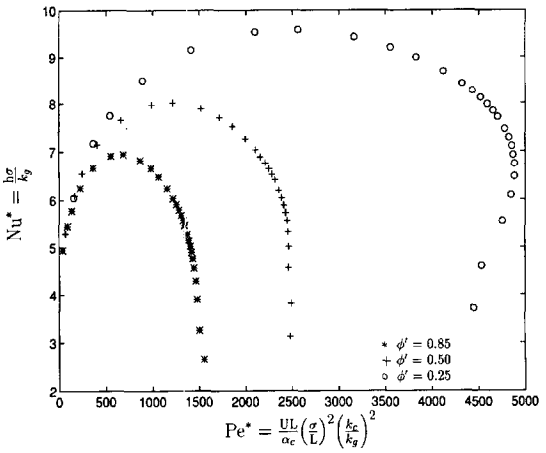

Fig. 18. The effect of varying the value of the specularity coefficient ϕ' on the variation of Nu^* with Pe^*. $e_p = 0.95$, $e_w = 0.50$, $\sigma = 3$ mm. Note that the symbols in the figure represent numerically calculated results and do not represent experimental data.

The theoretical studies also investigated the effect of varying the value of e_w. Lowering the value of e_w increased the dissipation of the fluctuation energy at the wall, leading to decreased values for the granular temperature and increased solid fractions due to inelastic clumping.

The theoretical solutions were extended to the convective heat transfer problem by solving the energy equation for the entire flow field assuming the total thermal conductivity to be the simple sum of a bulk molecular component and a kinetic component arising out of the streaming motion of the particles. Solutions were generated for both plug and sheared flows. Solutions for the plug flows, obtained by assuming a value of 0.01 for ϕ', provided values of Nu^* that were in good agreement with experimental data and the Sullivan–Sabersky model up to a value of $Pe^* \approx 600$. For higher values of Pe^*, the theoretical solutions predicted values for Nu^* that were higher than those observed in the experiments.

Three combinations of e_p and e_w were investigated in order to examine the convective heat transfer behavior in sheared granular flows. For all three cases, the profiles of Nu^* vs. Pe^* were found to exhibit a maximum for Nu^*, qualitatively similar to available experimental data. However, the theoretical solutions were unable to replicate the invariance of the value of Nu^* beyond the maximum, for increasing values of Pe^* as observed in the experiments. Also, the theoretical solutions could not replicate the shear induced enhancement of the heat transfer coefficient observed experimentally for values of slip velocities less than 4 cm s^{-1}. The value of e_w did not significantly affect the value of the heat transfer coefficients. The values of the heat transfer coefficients were found to decrease significantly with an increase in the value of the specularity coefficient ϕ'. Rougher walls lead to reduced values of solid fraction adjacent to the heated wall, thereby increasing the effective thickness of the interstitial fluid layer adjacent to the wall.

To investigate the influence of the streaming conductivity component on the heat transfer coefficients, comparisons were made amongst solutions generated for three different particle sizes. The results indicated that the streaming component became more significant as the particle size decreased.

In conclusion, it must be emphasized that the constitutive model, based on kinetic theory, utilized in this work incorporates many assumptions such as a 'continuum' approximation, an isotropic radial distribution function, and purely collisional interactions amongst particles that are not entirely appropriate in the context of most actual granular flows. However, in spite of these assumptions, such models are the only developed theoretical tools currently available that can qualitatively predict the shear-induced flow dilation and the accompanying anomalous convective heat transfer characteristics observed experimentally in flowing granular systems.

REFERENCES

1. Chapman, S. and Cowling, T. G., *The Mathematical Theory of Non-Uniform Gases*, 3rd edn. Cambridge University Press, 1971.
2. Ogawa, S., Multi-temperature theory of granular materials. *Proceedings of the U.S.–Japan Seminar on Continuum-Mechanical and Statistical Approaches in the Mechanics of Granular Materials*, 1978, pp. 208–217.
3. Campbell, C. S., Rapid granular flows. *Annual Review of Fluid Mechanics*, 1990, **22,** 57–92.
4. Savage, S. B. and Jeffrey, D. J., The stress tensor in a granular flow at high shear rates. *Journal of Fluid Mechanics*, 1981, **110,** 255–272.
5. Jenkins, J. T. and Savage, S. B., A theory for the rapid flow of identical, smooth, nearly elastic, spherical particles. *Journal of Fluid Mechanics*, 1983, **130,** 187–202.
6. Lun, C. K. K., Savage, S. B., Jeffrey, D. J. and Chep-

urniy, N., Kinetic theories for granular flow: inelastic particles in Couette flow and slightly inelastic particles in a general flow field. *Journal of Fluid Mechanics*, 1984, **140,** 223–256.
7. Jenkins, J. T. and Richman, M. W., Kinetic theory for plane flows of a dense gas of identical, rough, inelastic, circular disks. *Physics of Fluids*, 1985, **28,** 3485–3494.
8. Farrell, M., Lun, C. K. K. and Savage, S. B., A simple kinetic theory of granular flow of binary mixtures of smooth, inelastic, spherical particles. *Acta Mechanica*, 1986, **63,** 45–60.
9. Lun, C. K. K. and Savage, S. B., A simple kinetic theory for granular flow of rough, inelastic, spherical particles. *Journal of Applied Mechanics*, 1987, **54,** 47–53.
10. Jenkins, J. T. and Richman, M. W., Boundary conditions for plane flows of smooth, nearly elastic, circular disks. *Journal of Fluid Mechanics*, 1986, **171,** 53–69.
11. Lun, C. K. K., Kinetic theory for granular flow of dense, slightly inelastic, slightly rough spheres. *Journal of Fluid Mechanics*, 1991, **233,** 539–559.
12. Richman, M. W. and Oyediran, A. A., Grain size reduction in granular flows of spheres: the effects of critical impact energy. *Journal of Applied Mechanics*, 1992, **59,** 17–22.
13. Goldshtein, A. and Shapiro, M., Mechanics of collisional motion of granular materials. Part 1. General hydrodynamic equations. *Journal of Fluid Mechanics*, 1995, **282,** 75–114.
14. Hui, K., Haff, P. K., Ungar, J. E. and Jackson, R., Boundary conditions for high-shear grain flows, *Journal of Fluid Mechanics*, 1984, **145,** 223–233.
15. Richman, M. W., Boundary conditions based upon a modified Maxwellian velocity distribution for flows of identical, smooth, nearly elastic spheres. *Acta Mechanica*, 1988, **75,** 227–240.
16. Richman, M. W. and Marciniec, R. P., Gravity-driven granular flows of smooth, inelastic spheres down bumpy inclines. *Journal of Applied Mechanics*, 1990, **112,** 1036–1043.
17. Johnson, P. C. and Jackson, R., Frictional–collisional constitutive relations for granular materials, with application to plane shearing. *Journal of Fluid Mechanics*, 1987, **176,** 67–93.
18. Jenkins, J. T., Boundary conditions for rapid granular flow: flat, frictional walls. *Journal of Applied Mechanics*, 1992, **59,** 120–127.
19. Sun, J. and Chen, M. M., A theoretical analysis of heat transfer due to particle impact. *International Journal of Heat and Mass Transfer*, 1988, **31,** 205–214.
20. Schlunder, E. U., Particle heat transfer. *Proceedings of the Seventh International Heat Transfer Conference*. Munich, Hemisphere Pub. Co., 1982.
21. Sullivan, W. N. and Sabersky, R. H., Heat transfer to flowing granular media. *International Journal of Heat and Mass Transfer*, 1975, **18,** 97–107.
22. Spelt, J. K., Brennen, C. E. and Sabersky, R. H., Heat transfer to flowing granular material. *International Journal of Heat and Mass Transfer*, 1982, **25,** 791–796.
23. Patton, J. S., Sabersky, R. H. and Brennen, C. E., Convective heat transfer to rapidly flowing granular materials. *International Journal of Heat and Mass Transfer*, 1986, **29,** 1263–1269.
24. Ahn, H., Experimental and analytical investigations of granular materials : shear flow and convective heat transfer. Ph.D. thesis, California Institute of Technology, Pasadena, 1989.
25. Natarajan, V. V. R., Material and thermal transport in vertical granular flows. Ph.D. thesis, California Institute of Technology, Padadena, 1997.
26. Natarajan, V. V. R. and Hunt, M. L., Heat transfer in vertical granular flows. *Experimental Heat Transfer*, 1997, **10**(2), 89–107.
27. Louge, M., Yusof, J. M. and Jenkins, J. T., Heat transfer in the pneumatic transport of massive particles. *International Journal of Heat and Mass Transfer*, 1993, **36**(2), 265–275.
28. Boateng, A. A. and Barr, P. V., A thermal model for the rotary kiln including heat transfer within the bed. *International Journal of Heat and Mass Transfer*, 1996, **39**(10), 2131–2147.
29. Hsiau, S. S. and Hunt, M. L., Kinetic theory analysis of flow-induced particle diffusion and thermal conduction in granular material flows. *Transactions of ASMEC: Journal of Heat Transfer*, 1993, **115,** 541–548.
30. Hunt, M. L., Discrete element simulations for granular material flows: effective thermal conductivity and self-diffusivity. *International Journal of Heat and Mass Transfer*, 1997, **40**(13), 3059–3068.
31. Gelperin, N. I. and Einstein, V. G., Heat transfer in fluidized beds. In *Fluidization*, ed. J. F. Davidson and D. Harrison. Academic Press, London and New York, 1971, pp. 471–568.
32. Natarajan, V. V. R., Hunt, M. L. and Taylor, E. D., Local measurements of velocity fluctuations and diffusion coefficients for a granular material flow. *Journal of Fluid Mechanics*, 1995, **304,** 1–25.
33. Johnson, P. C., Nott, P. and Jackson, R., Frictional–collisional equations of motion for particulate flows and their application to chutes. *Journal of Fluid Mechanics*, 1990, **210,** 501–535.
34. Hsiau, S. S., Shear induced transport properties of granular material flows. Ph.D. thesis, California Institute of Technology, Pasadena, 1993.
35. Foerster, S. F., Louge, M. Y., Chang, H. and Allia, K., Measurements of the collision properties of small spheres. *Physics of Fluids*, 1994, **6**(3), 1108–1115.
36. Drake, T. G., Granular flow: physical experiments and their implications for microstructural theories. *Journal of Fluid Mechanics*, 1991, **225,** 121–152.
37. Patankar, S. V., *Handbook of Numerical Heat Transfer*, ed. E. M. Sparrow, W. J. Minkowycz, G. E. Schneider and R. H. Pletcher, Chap. 6. John Wiley and Sons, 1988, pp. 215–227.
38. Patankar, S. V., *Numerical Heat Transfer and Fluid Flow*. Chap. 5. McGraw-Hill, 1980, pp. 79–109.